

**PHASE CHAOS AND MULTISTABILITY  
IN THE DISCRETE KURAMOTO MODEL**

**ФАЗОВИЙ ХАОС ТА МУЛЬТИСТІЙКІСТЬ  
У ДИСКРЕТНІЙ МОДЕЛІ КУРАМОТО**

**V. Maistrenko, A. Vasylenko**

*Inst. Math. Nat. Acad. Sci. Ukraine  
Tereshchenkivska St. 3, Kyiv, 01601, Ukraine*

**Yu. Maistrenko**

*Inst. Math. Nat. Acad. Sci. Ukraine  
Tereshchenkivska St. 3, Kyiv, 01601, Ukraine  
and  
Inst. Medicine  
Research Centre Jülich, 52425, Jülich, Germany*

**E. Mosekilde**

*Techn. Univ. Denmark  
DK-2800, Kongens Lyngby, Denmark*

*The paper describes the appearance of a novel, a high-dimensional chaotic regime, called phase chaos, in the discrete Kuramoto model of globally coupled phase oscillators. This type of chaos is observed at small and intermediate values of the coupling strength. It is caused by the nonlinear interaction of the oscillators, while the individual oscillators behave periodically when left uncoupled. For the four-dimensional discrete Kuramoto model we outlined the region of the phase chaos in the parameter plane and distinguished the region where the phase chaos coexists with other periodic attractors, and demonstrate, in addition, that the transition to the phase chaos takes place through the torus destruction scenario.*

*Описано виникнення нового багатовимірного хаотичного режиму, який називають фазовим хаосом, у дискретній моделі Курамото глобально зв'язаних фазових осциляторів. Цей тип хаосу спостерігають при малих та середніх значеннях параметра зв'язку. Він спричиняється нелінійною взаємодією осциляторів, тоді як поведінка незв'язаних індивідуальних осциляторів є періодичною. Для чотиривимірної дискретної моделі Курамото окреслено область фазового хаосу в площині параметрів, виділено область, де фазовий хаос співіснує з іншими періодичними аттракторами, та продемонстровано, що перехід до фазового хаосу відбувається через сценарій руйнування тора.*

**1. Introduction.** Unraveling the collective behavior of a group of interacting oscillators represents a challenging problem that arises in many areas of science and technology [1–5]. Examples from biology and the lifesciences are the generation of cyclic AMP pulsors in slime mold cultures of *Dictyostelium discoideum* [6], the propagation of waves of cytoplasmic  $\text{Ca}^{2+}$  across islets of bursting pancreatic cells [7], the newly discovered synchronization of metabolic processes in suspensions of yeast cells [8], and the entrainment of the pressure and flow regulation between neighboring nephrons in the kidney [9]. Examples from physics, chemistry and engi-

neering have been published, for instance, by Hadley et al. [10], Kiss et al. [11] and Rulkov [12]. Problems of this type have been investigated from many different points of view. Postnov et al. [13], for instance, have suggested a mechanism for the development of high-order chaos and, more recently, De Monte et al. [14] have established an order parameter expansion by which the mean field dynamics of a population of oscillators with parameter diversity and global coupling can be described in terms of a few macroscopic degrees of freedom.

Pulse- and phase-coupled oscillators constitute a paradigmatic class of interacting dynamical units. Over the years, particular emphasis has been paid to the so-called Kuramoto system [1, 4], i.e., to models of coupled phase oscillators. Such models represent the simplest approach to the coupled oscillator problem, namely an approach in which the individual oscillator is described by a single variable, the value of its instantaneous phase. Nonetheless, models of this type have been surprisingly effective in designing new ways to desynchronize clusters of brain cells in patients with Parkinsonian and other forms of tremor [15, 16]. Only recently, investigations have begun based on more physiologically realistic nerve and glia cell models. However, the dynamics of the finite-dimensional Kuramoto system is still far from being understood in detail, and one of the recent results of the above neurological applications of the model was the observation of a new high-dimensional chaotic phenomenon called *phase chaos* [17]. Motivated by these results, the present paper considers a time-discrete version of the Kuramoto model which has some features in common with the continuous-time system, but also manifests some important differences [18, 19].

Typical questions that arise in the investigations of complex dynamical systems are related to the collective dynamics of an ensemble of oscillators (such as synchronization, clustering or the appearance of chaos and higher-dimensional dynamics), how the dynamics can be changed with varying the system parameters, and the bifurcations that lead to the appearance of different dynamical states. In the present paper we concentrate on the studying the characteristics of phase chaos and the mechanisms by which this form of chaos appears.

The paper is organized as follows. In Section 2 we introduce the  $N$ -dimensional and 4-dimensional discrete Kuramoto models of globally coupled phase oscillators and describe the change of variables which allows us to reduce the dimension of the system by one. The following sections are devoted to the study of the four-dimensional Kuramoto model and the corresponding three-dimensional map in the case when the frequencies of the individual oscillators are distributed equidistantly over some interval. By this condition we reduce the number of system parameters. In Section 3 we present the regions of stability of periodic orbits in the plane of system parameters, discuss phenomenon of multistability and show some characteristic phase portraits of the system. In Section 4 we describe the structure of the phase-locking regions for the Poincaré map of our three-dimensional system and, using the method of Lyapunov exponents to detect the chaotic behavior, we outline the region of phase chaos in the parameter plane. In Section 5 the mechanism of appearance of the phase chaos is described in more detail, and we show how this form of chaos arises through a torus destruction scenario.

**2. The model.** Let us consider the discrete Kuramoto model of  $N$  globally coupled phase oscillators

$$\psi_i^{(n+1)} = \psi_i^{(n)} + \omega_i + \frac{K}{N} \sum_{j=1}^N \sin(\psi_j^{(n)} - \psi_i^{(n)}), \quad i = \overline{1, N}, \quad (1)$$

where  $N \in \mathbb{Z}$  and  $n = 0, 1, \dots$  represents the discrete time,  $\psi_i$  are the phase variables,  $\omega_i$  —

the natural frequencies of individual oscillators and  $K > 0$  is the coupling parameter.

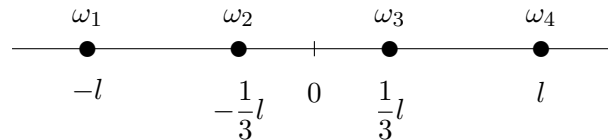
Such a discrete-time Kuramoto model has some features in common with the continuous-time system [16–18]. However, in general, the discrete-time models exhibit more complicated and rich dynamics than the continuous-time ones.

For the time-continuous Kuramoto model it was found that systems of at least  $N \geq 4$  display a novel type of chaotic behaviour called *phase chaos* [17]. The present paper considers the four-dimensional discrete-time Kuramoto system, as an extension of our recent work [19], where the same system with  $N = 2$  and 3 was investigated.

In this work we consider the four-dimensional discrete Kuramoto model and the case of the main resonance,  $\omega_i$  are distributed equidistantly in the interval  $[-l; l]$ ,  $l > 0$  :

$$\psi_i^{(n+1)} = \psi_i^{(n)} + \omega_i + \frac{K}{4} \sum_{j=1}^4 \sin(\psi_j^{(n)} - \psi_i^{(n)}), \quad i = \overline{1, 4}, \tag{2}$$

where  $\omega_1 = -l, \omega_2 = -\frac{1}{3}l, \omega_3 = \frac{1}{3}l, \omega_4 = l$  :



When studying the collective dynamics and interaction of the phase oscillators, it is useful to consider differences of the individual phase variables. Indeed, introducing new phase difference variables:

$$\varphi_i = \psi_{i+1} - \psi_i, \quad i = \overline{1, N-1}, \tag{3}$$

we can reduce the dimension of the system (1) by one. The effective dynamics then take place on the torus  $\mathbb{T}^{N-1}$ .

**Three-dimensional system.** After change of the variables (3) in the system (1) the dynamics are governed by the following three-dimensional system:

$$\begin{aligned} \varphi_1^{(n+1)} &= \varphi_1^{(n)} + \Delta_1 - \frac{K}{4} \left( 2 \sin \varphi_1^{(n)} + \sin(\varphi_1^{(n)} + \varphi_2^{(n)}) + \sin(\varphi_1^{(n)} + \varphi_2^{(n)} + \varphi_3^{(n)}) - \right. \\ &\quad \left. - \sin \varphi_2^{(n)} - \sin(\varphi_2^{(n)} + \varphi_3^{(n)}) \right), \\ \varphi_2^{(n+1)} &= \varphi_2^{(n)} + \Delta_2 - \frac{K}{4} \left( 2 \sin \varphi_2^{(n)} + \sin(\varphi_1^{(n)} + \varphi_2^{(n)}) + \sin(\varphi_2^{(n)} + \varphi_3^{(n)}) - \right. \\ &\quad \left. - \sin \varphi_1^{(n)} - \sin \varphi_3^{(n)} \right), \\ \varphi_3^{(n+1)} &= \varphi_3^{(n)} + \Delta_3 - \frac{K}{4} \left( 2 \sin \varphi_3^{(n)} + \sin(\varphi_2^{(n)} + \varphi_3^{(n)}) + \sin(\varphi_1^{(n)} + \varphi_2^{(n)} + \varphi_3^{(n)}) - \right. \\ &\quad \left. - \sin \varphi_2^{(n)} - \sin(\varphi_1^{(n)} + \varphi_2^{(n)}) \right), \end{aligned} \tag{4}$$

where the variables  $\varphi_1, \varphi_2, \varphi_3$  are given by (3), and frequencies differences  $\Delta_i = \omega_{i+1} - \omega_i, i = 1, 2, 3$ . From the form of the equations one can conclude that in the case  $\Delta_1 = \Delta_3$  the system (4) has a symmetric invariant manifold  $\mathcal{M} = \{\varphi_1 = \varphi_3\}$ .

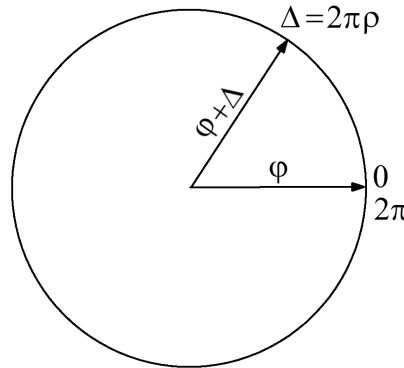


Fig. 1. Sketch of the dynamics of the circle map (5).

We will consider the case of main resonance  $\Delta_i = \Delta$ ,  $i = 1, 2, 3$ . When  $K = 0$  the dynamics are determined by the one-dimensional circle map

$$\varphi^{(n+1)} = \varphi^{(n)} + \Delta \pmod{2\pi}, \quad n \geq 0. \quad (5)$$

Here  $\Delta = \frac{2}{3}l$  according to our designations. This map describes a simple rotation, its dynamics are characterized by the rotation number  $\rho = \lim_{n \rightarrow \infty} \frac{\varphi^{(n)} - \varphi^{(0)}}{2\pi n} = \frac{\Delta}{2\pi}$ , see Fig. 1. If  $\rho$  is rational, i.e.,  $\rho = \frac{p}{q}$ , then all trajectories are periodic with period  $T = q$ . If  $\rho$  is irrational, all trajectories are quasiperiodic.

**3. Phase-locking regions.** When adding perturbation  $KF$  to the map (5):

$$\varphi^{(n+1)} = \varphi^{(n)} + \Delta + KF(\varphi^{(n)}) \pmod{2\pi}, \quad (6)$$

regions of periodicity corresponding to rational rotation numbers  $\frac{p}{q}$  emerge from the points  $\left(\frac{p}{q}; 0\right)$  in the parameter plane  $(\Delta; K)$ . Such regions are also called phase-locking regions, regions of synchronization or Arnol'd tongues.

Three-dimensional discrete Kuramoto model (4) can be considered as a perturbation of the map (5), where  $K \geq 0$  is a parameter of the perturbation. We find that for  $K > 0$  the system (4) can exhibit periodic, quasiperiodic and chaotic dynamics. To overview the system dynamics for different values of the parameters, we have determined main parameter regions of existence and stability of the orbits in the plane  $(l, K)$ . Fig. 2 depicts the widest Arnol'd tongues as well as the region of phase chaos, which will be discussed in more detail in the following sections.

For the parameter of discreteness  $l$ , the following relation takes place:

$$\Delta = \frac{2}{3}l = 2\pi\rho.$$

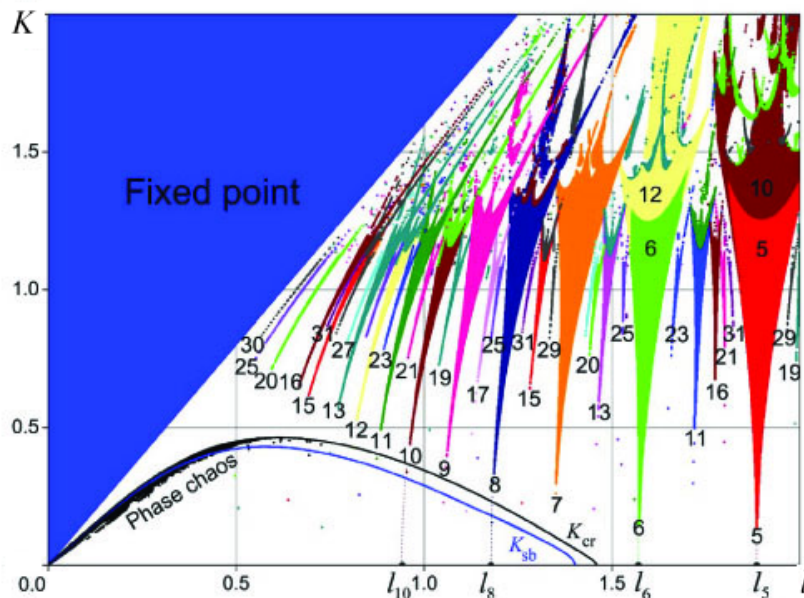


Fig. 2. Regions of stability for the main periodic orbits of the three-dimensional system (4). Numbers denote periods of the stable orbits inside the Arnol'd tongues; these cycles lose the transverse stability in the bifurcation  $K_{sb}$  — symmetry-breaking; the curve  $K_{cr}$  shows where boundary crisis for the chaotic attractor takes place;  $K$  is the coupling parameter, and  $l$  is a measure of the spread in natural frequencies.

As shown in Fig. 2 the Arnol'd tongues of the rotation numbers  $\rho = \frac{p}{q}$  emanate from the points  $l_q = \frac{3}{2} 2\pi\rho = 3\pi\frac{p}{q}$ . In the figure, we denoted the tongues of the  $q$ -periodic orbits with the corresponding numbers, and for some of the tongues we have shown points  $l_q$  of their origin on the axis  $l$ . For example, the region of stability of the periodic orbit with period 5 corresponds to the rotation number  $\rho = \frac{1}{5}$  and emanates from the point  $l_5 = 3\pi\frac{1}{5} \approx 1.885$ . Analogously  $l_6 = 3\pi\frac{1}{6} \approx 1.57$ ;  $l_8 = 3\pi\frac{1}{8} \approx 1.178$ ;  $l_{10} = 3\pi\frac{1}{10} \approx 0.94$ . As we have found, periodic orbits, existing in these phase-locking regions, belong to the diagonal  $\mathcal{M} = \{\varphi_1 = \varphi_3\}$ . Two phase portraits in Fig. 3 (a, b) show typical attractors inside the diagonal. With decrease in  $K$ , the attractor in the diagonal  $\mathcal{M}$  loses its transverse stability at the bifurcation curve  $K_{sb}$  — symmetry-breaking. The Arnol'd tongues go down to the axis  $l$ , but the periodic orbits which are stable inside  $\mathcal{M}$ , are no longer stable transversally to  $\mathcal{M}$ . At the same time, for all  $K < K_{cr}$  other attractors exist outside the manifold  $\mathcal{M}$ , an example is shown in Fig. 3 (c). In the parameter region between  $K_{sb}$  and  $K_{cr}$ , we have multistability: two attractors, one inside  $\mathcal{M}$  and another outside  $\mathcal{M}$  coexist. This can be illustrated with graphs of the Lyapunov exponents for these attractors, see Fig. 4, in this case the attractor outside  $\mathcal{M}$  is chaotic, and we will discuss such dynamics in more detail later.

The structure of the Arnol'd tongues is standard, and they are arranged in accordance with the rule of Fibonacci numbers. The widest tongues belong to the first level and their rotation numbers are ordered according to the period-adding rule. In between every pair of the tongues of the rotation numbers  $\frac{1}{q}$  and  $\frac{1}{q+1}$  there is a smaller tongue of

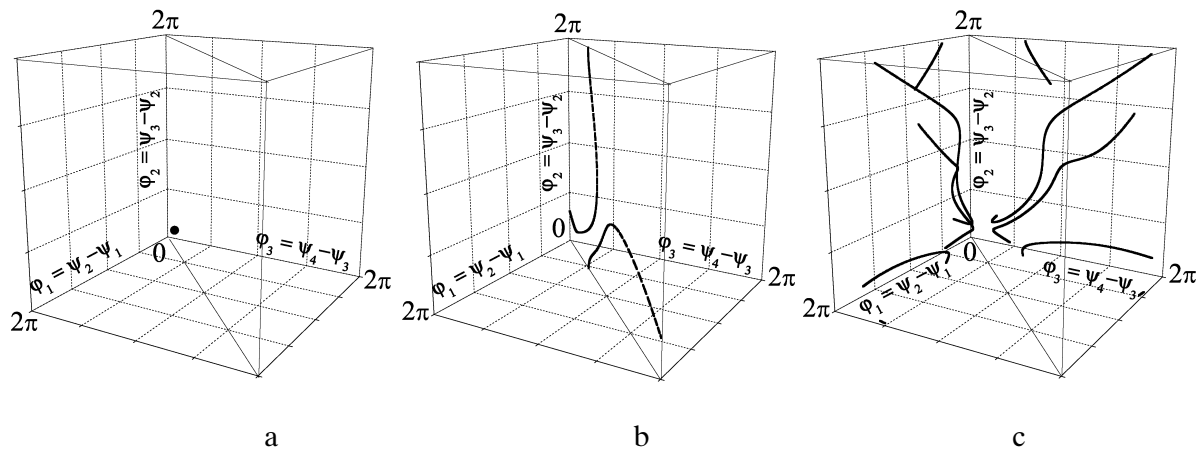


Fig. 3. Phase portraits of the three-dimensional system (4): (a) fixed point of the system (4) inside  $\mathcal{M}$ ,  $l = 0.126$ ,  $K = 0.2$ ; (b) quasiperiodic trajectory of (4) inside  $\mathcal{M}$ , it intersects the plane  $\varphi_2 = 0$  only once this intersection is the fixed point of the Poincaré map,  $l = 0.14$ ,  $K = 0.2$ ; (c) quasiperiodic torus for the system (4) outside  $\mathcal{M}$ , stable periodic orbit of the period 4 for the Poincaré map,  $l = 0.08623$ ,  $K = 0.1$ .

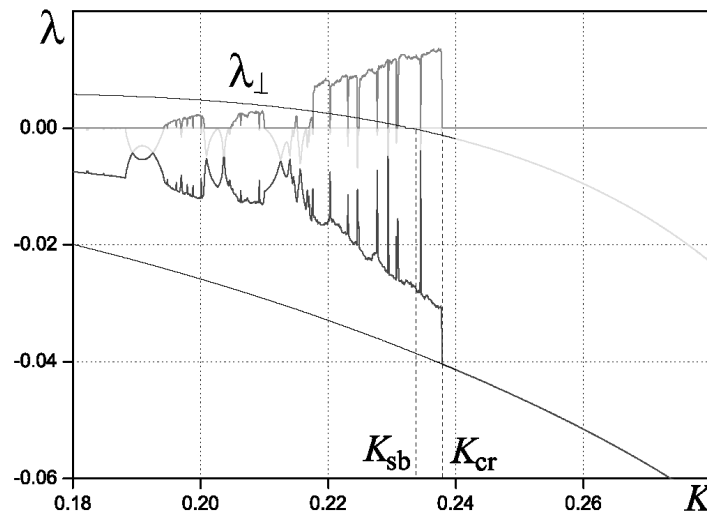


Fig. 4. Forward and backward calculations of the Lyapunov exponents for the attractors inside and outside the manifold  $\mathcal{M}$ ,  $l = 0.2$ .

the second level of the rotation number  $\frac{2}{2q+1}$ ; between the tongues corresponding to  $\frac{1}{q}$  and  $\frac{2}{2q+1}$  there is a tongue of the third level with  $\rho = \frac{3}{3q+1}$  and so on. Boundaries of the tongues are curves of saddle-node bifurcations for the periodic orbits existing inside the tongues. The dynamics of the system (4) are one-to-one (invertible) for all  $0 < K \leq 1$ . For the values of  $K$  greater than 1, the dynamics become non-invertible and transition to chaos takes place through the period-doubling cascades.

**Construction of the Poincaré map.** To further simplify the analysis we will use the classical idea of Poincaré, who proposed a method to reduce the studies of continuous-time systems by considering the associated Poincaré maps. For an  $N$ -dimensional flow the core of this method lies in considering respective discrete dynamics on some  $(N - 1)$ -dimensional surface transverse to the vector field. This method allows one to reduce the dimension of the system and it also provides a useful display of the global dynamics of the system. A similar approach can be applied for studying discrete-time models that exhibit quasiperiodic behavior. For the parameter values that correspond to quasiperiodic or chaotic trajectories we can define the Poincaré map by considering only the intersections of the trajectories with some particular plane.

For the three-dimensional system (4) we choose to analyze the Poincaré map on the torus section  $\varphi_2 = 0$ . As shown in Fig. 2 there exist a wide region of stability of the fixed point and many regions corresponding to stability of some periodic orbits. But for smaller values of coupling  $K$  the Arnol'd tongues are very narrow, and quasiperiodic trajectories prevail. The region of quasiperiodicity is coloured in white on the figure, and for the corresponding values of parameters we will apply the method of Poincaré. Our main interest is in considering the parameter values in the lower left corner of Fig. 2, since it is in this region that we find chaotic behavior unexpectedly.

As shown in Fig. 2 we have found that the system exhibits chaotic behavior for unusually small values of the coupling  $K$ , far away from the region where the Arnol'd tongues overlap due to non-invertibility of the map (4), that appears for  $K > 1$ , which causes the well-known chaoticity observed, for instance, in the sine circle map [19, 20]. Following [17], we will call this type of chaos, which appears for small  $K$  and  $l$ , — *phase chaos*. The key to understanding the appearance of phase chaos in this region can be found by considering the dynamics of the Poincaré map.

To get a better insight into the system dynamics several phase portraits of the three-dimensional system (4) are depicted in Fig. 3. Fig. 3 (a) corresponds to existence of a stable fixed point for the system (4). Fig. 3 (b, c) show the cases when the attractor of the system is an invariant curve, and the intersection of this curve with the plane  $\varphi_2 = 0$  implies the existence of the fixed or periodic points for the Poincaré map considered.

**4. Arnol'd tongues for the Poincaré map.** To consider the transition to phase chaos in more detail let us study the occurrence of periodic orbits for the Poincaré map. The general picture of the main tongues is presented in Fig. 5 and, enlarged, in Fig. 6. In these figures, the stability regions of different periodic orbits are shown. The existence of an Arnol'd tongue for some  $m$ -periodic orbit of the Poincaré map signifies the existence of an invariant curve for the three-dimensional system (4), and this curve intersects the plane  $\varphi_2 = 0$  in  $m$  points, as illustrated by phase portraits in Fig. 3. Phase chaos occurs in the region where the Arnol'd tongues for the Poincaré map intersect and overlap each other. The chaotic attractor is destroyed in a boundary crisis which is marked with the bifurcation curve  $K_{cr}$  in Fig. 5.

The structure and the disposition of the tongues are shown in more detail in Fig. 6. These regions are ordered in a standard way: the widest tongues are located in accordance with a period-adding rule. In between every pair of tongues with periods  $p$  and  $p + 1$  there is a smaller tongue for the period  $2p + 1$ , between the regions for periods  $p$  and  $2p + 1$  there is a tongue for the period  $3p + 1$  and so on. The boundaries of the tongues are curves of saddle-node bifurcations and in the top of the tongues, where period-doubling cascades occur, one can observe the transition to chaotic behavior.

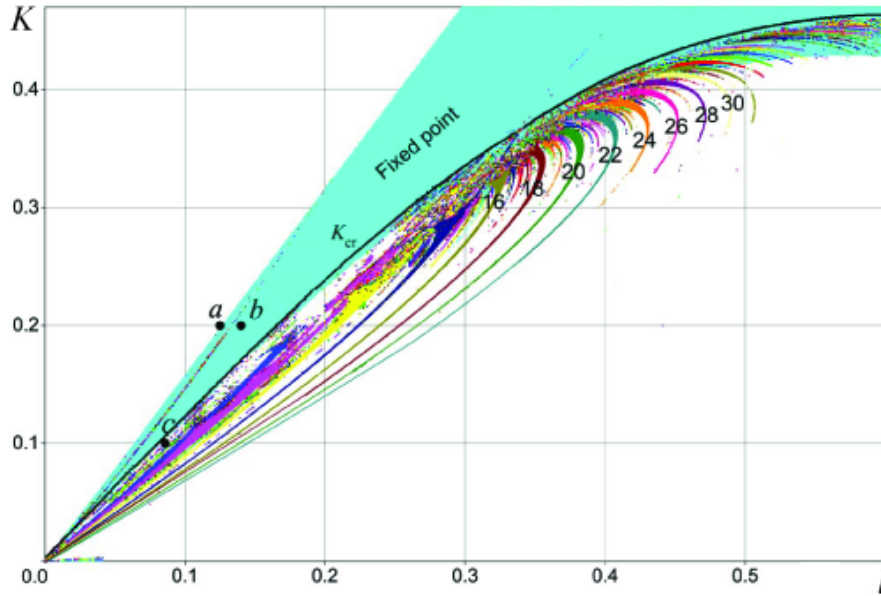


Fig. 5. Some of the Arnol'd tongues for the Poincaré map in the region of appearance of phase chaos; the numbers show the periods of the periodic orbits; the bifurcation curve  $K_{cr}$  denotes the boundary crisis of the chaotic attractor; the points  $a-c$  correspond to the parameter values for the phase portraits in Fig. 3.

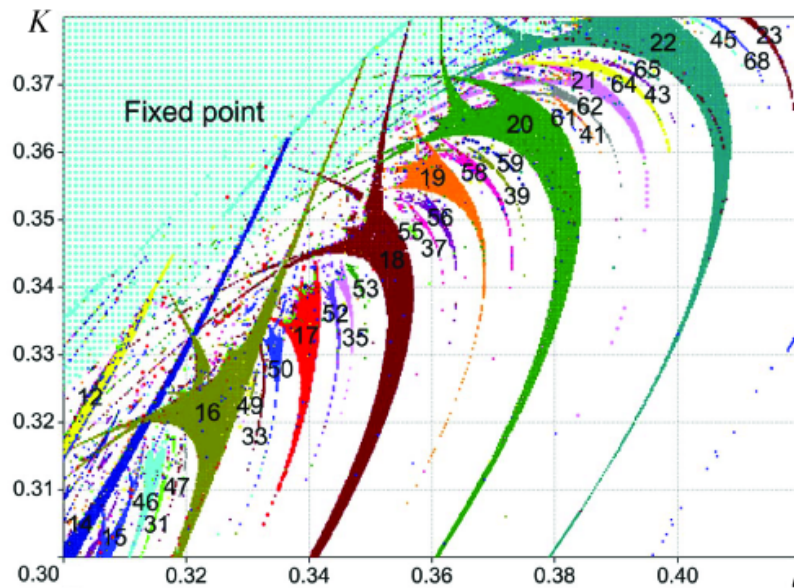


Fig. 6. Structure of the phase-locking regions for the Poincaré map of the system (4); the numbers denote the periods of the periodic orbits for the corresponding tongues.

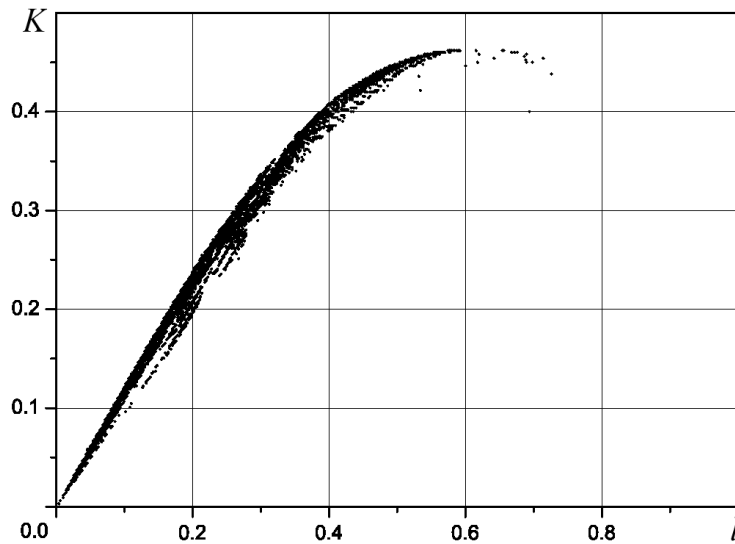


Fig. 7. Region of phase chaos, outlined with the method of Lyapunov exponents by the condition  $\lambda_{\max} \geq 0.001$ ; for comparison, the zero-valued Lyapunov exponent takes values of the order 0.0001.

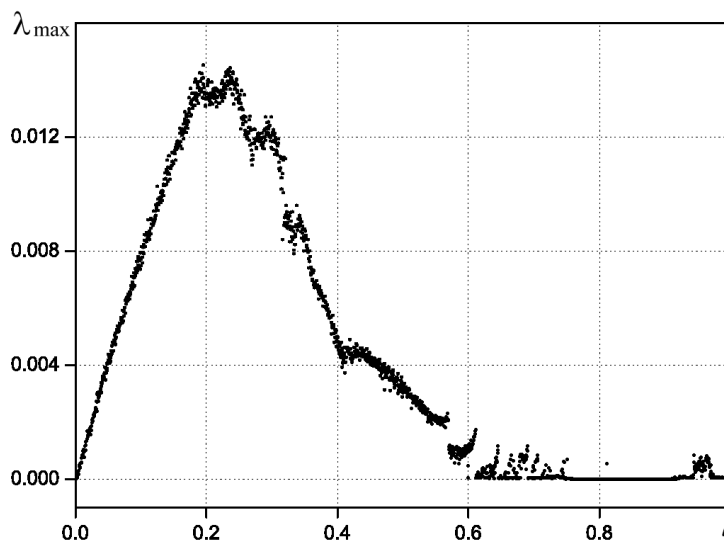


Fig. 8. Maximum with  $K$  of the maximal Lyapunov exponents in the region of appearance of the phase chaos.

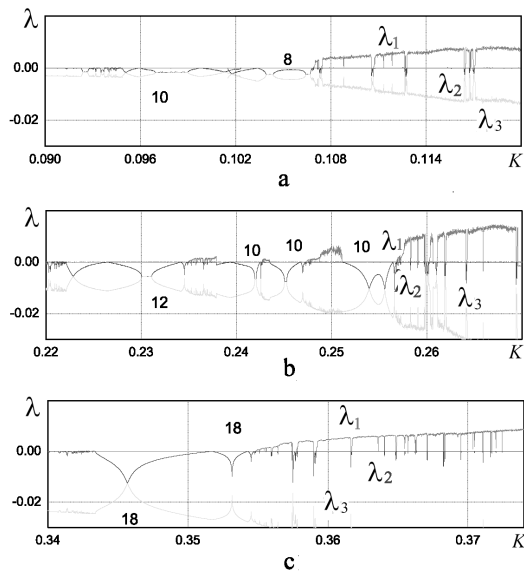


Fig. 9. Lyapunov exponents of the system (4),  $l = 0.1$  (a), 0.23 (b), 0.35 (c); the numbers denote the periods for the tongues crossed while calculating the exponents.

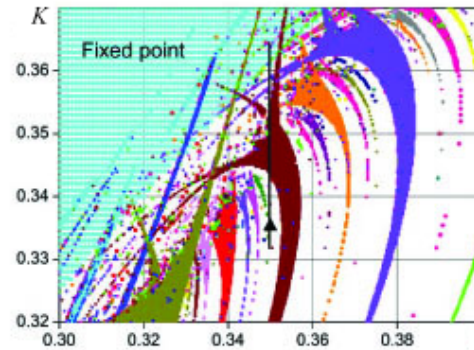


Fig. 10. Parameter region where the transition to phase chaos occurs; different regions of stability of periodic orbits for the Poincaré map, the arrow shows the parameter values for which the Lyapunov exponents in the last graph of Fig. 9 were calculated.

**Lyapunov exponents and phase chaos.** To detect the chaotic, quasiperiodic or periodic regimes of the system dynamics we calculate the Lyapunov exponents. The system has three Lyapunov exponents with one of them being always equal to zero. The maximal exponent  $\lambda_1$ , when it becomes positive, signals the appearance of phase chaos. The region of parameter values where phase chaos occurs is shown in Fig. 7. To outline this region we used the criteria  $\lambda_{\max} \geq 0.001$ , considering all the smaller values to be zero. It is also interesting to observe how the value of the maximal Lyapunov exponent varies in the parameter region where the phase chaos occurs. For the range of  $l$ -values we considered such values of  $K$  where  $\lambda_1$  is positive and compared  $\lambda_1$  for different  $K$  in order to find the maximum. The resulting graph is shown in Fig. 8. One can see the correspondance between the region of phase chaos and the dynamics of the Lyapunov exponents.

Fig. 9 shows several graphs of the Lyapunov exponents for the parameter values that correspond to appearance of chaotic attractors. As shown, the maximal exponent reaches the values of order 0.01, while the zero Lyapunov exponent takes values of order 0.0001. Fig. 10 shows the main Arnol'd tongues in the region where the Lyapunov exponents were calculated. The arrow corresponds to the third graph in Fig. 9. Fig. 10 shows that if we increase the parameter  $K$  then the transition to chaos occurs after leaving the tongue of periodicity.

The region of phase chaos in the  $(l, K)$ -parameter plane is found to possess a complicated topological structure due to multiple intersections with tongues of periodicity, causing multistability and coexistence of the chaotic behavior with the phase locked states.

**5. By torus destruction to phase chaos.** Let us finally consider the types of phase dynamics that are typical for our system and precede the transition to phase chaos. Fig. 11 defines several points (a – f) in the parameter plane, which were chosen for our examination, and Fig. 12

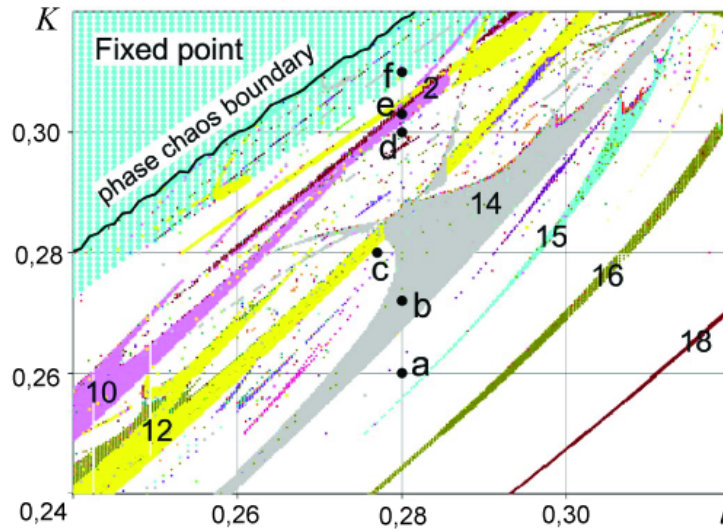


Fig. 11. Some of the mode-locking regions near the transition to phase chaos. Points  $a-f$  correspond to the parameter values for the phase portraits in Fig. 12. Point  $a$  is situated in a region of quasiperiodic dynamics, point  $b$  — in a region with period-14 dynamics, and  $c$  — in a parameter region where the torus is wrinkled. The point  $f$  falls in a region of fully developed phase chaos. The black boundary shows the bifurcation line that corresponds to the boundary crisis of the chaotic attractor.

demonstrates the phase portraits for the corresponding parameter values. Between the phase-locking regions there exists a quasiperiodic attractor for the Poincaré map. This is illustrated in Fig. 12 ( $a$ ). With the change of the parameters the quasiperiodic torus becomes wrinkled, and the transition to chaos takes place, as shown in Fig. 12 ( $c$ ). This confirms that phase chaos appears through the torus destruction scenario. With further variation of the parameters, wrinkles and nonsmoothness spread along the torus, and it breaks up into a fractal or strange structure.

The torus destruction scenario applies to smooth systems and to systems that can be represented by two-dimensional invertible maps. It is a common scenario for the loss of smoothness in systems that display quasiperiodicity and phase locking [20].

For the parameter values inside the Arnol'd tongues the behavior on the plane  $\varphi_2 = 0$  is periodic. Examples of the periodic orbits are depicted in Figs. 12 ( $b, e$ ), and Figs. 12 ( $d, f$ ) show the phase portraits in the case of the chaotic behavior. As discussed earlier, the phase chaos can coexist with some other attractors, and in Fig. 12 ( $f$ ) one can see the fixed point coexisting with the chaotic attractor.

**6. Conclusions.** Phase chaos is a novel phenomenon in nonlinear systems of coupled oscillators [17]. In the present paper we investigate the appearance of this type of chaos in the discrete Kuramoto model of globally coupled phase oscillators. The peculiarity of the phase chaos is that this type of chaotic behavior takes place even for very small values of the coupling parameter. When changing the coupling from zero one would intuitively expect emergence of a coherence among the oscillators, but we find chaotic behaviour there. Nonlinear interactions of the oscillators cause chaoticity of the collective phase dynamics even for those parameter values which correspond to periodic behaviour of the uncoupled individual oscillators. The same type

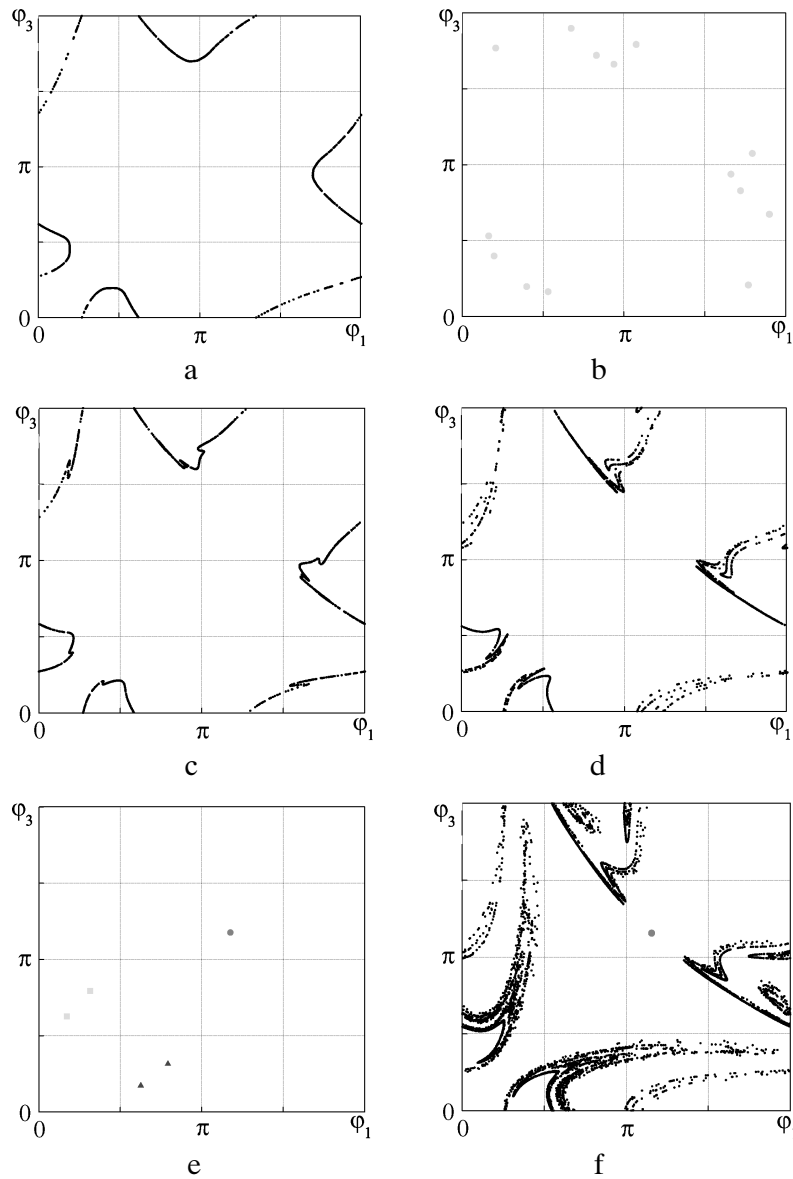


Fig. 12. Phase portraits obtained for different parameter values corresponding to the points  $a - f$  in the Fig. 11: (a) shows a quasiperiodic torus for  $l = 0.28$  and  $K = 0.26$ , (b) a stable periodic orbit of period 14,  $l = 0.28$ ,  $K = 0.272$ , (c) phase chaos,  $\lambda_1 \approx 0.0026$ ,  $l = 0.277$ ,  $K = 0.28$ , (d) phase chaos,  $\lambda_1 \approx 0.007$ ,  $l = 0.28$ ,  $K = 0.3$ , (e) two stable periodic orbits of period 2, coexisting with a fixed point,  $l = 0.28$ ,  $K = 0.303$ , (f) phase chaos,  $\lambda_1 \approx 0.01$ , and fixed point,  $l = 0.28$ ,  $K = 0.31$ .

of chaos has been found in other systems both regular and chaotic [21, 22], and this allows us to conclude that phase chaos is, probably a common phenomenon of networks of very different nature. However, the detailed analysis of this phenomena has not yet been taken, and as a significant achievement, in the present paper we present the parameter region of the phase chaos existence, region of multistability and the regions of existence of the periodic orbits which help to understand the appearance of the chaotic behavior.

In this work we find typicalness of phase chaos for a discrete analog of the Kuramoto model, and analyse how it depends on a new parameter  $l$  induced by discreteness. We describe the structure of the Arnol'd tongues and show how this form of chaos arises through a torus destruction scenario.

1. *Kuramoto Y.* Chemical oscillations, waves and turbulence. — Berlin: Springer, 1984. — 163 p.
2. *Haken H.* Principles of brain functioning. — Berlin; Heidelberg: Springer, 1996. — 348 p.
3. *Blekhman I.* Synchronization in science and technology. — New York: Asme Press, 1988. — 350 p.
4. *Pikovsky A., Rosenblum M., Kurths J.* Synchronization — a universal concept in nonlinear sciences. — Cambridge: Cambridge Univ. Press, 2001. — 432 p.
5. *Mosekilde E., Maistrenko Yu., Postnov D.* Chaotic synchronization. Application to living systems. — New Jersey: World Sci., 2002. — 430 p.
6. *Goldbeter A., Wurster B.* Regular oscillations in suspensions of a putatively chaotic mutant of *Dictyostelium discoideum* // *Experientia*. — 1989. — **45**. — P. 363–365.
7. *Gylfe E., Grapenqviesser E., Hillman B.* Propagation of cytoplasmic  $Ca^{2+}$  oscillations in clusters of pancreatic  $\beta$ -cells exposed to glucose // *Cell Calcium*. — 1991. — **12**. — P. 229–240.
8. *Danø S., Sørensen P. G., Hynne F.* Sustained oscillations in living cells // *Nature*. — 1999. — **402**. — P. 320–322.
9. *Holstein-Rathlou N. -H., Yip K. -P., Sosnovtseva O. V., Mosekilde E.* Synchronization phenomena in nephron–nephron interaction // *Chaos*. — 2001. — **11**. — P. 417–426.
10. *Hadley P., Beasley M. R., Wiesenfeld K.* Phase locking of Josephson-junction series arrays // *Phys. Rev. B*. — 1988. — **38**. — P. 8712–8719.
11. *Kiss I. Z., Zhai Y., Hudson J. L.* Emerging coherence in a population of chemical oscillators // *Science*. — 2002. — **296**. — P. 1676–1678.
12. *Rulkov N. F.* Images of synchronized chaos: experiments with circuits // *Chaos*. — 1996. — **6**. — P. 262–279.
13. *Postnov D. E., Balanov A. G., Sosnovtseva O. V., Mosekilde E.* Chaotic hierarchy in high dimensions // *Int. J. Mod. Phys. B*. — 2000. — **14**. — P. 2511–2527.
14. *De Monte S., d'Ovidio F., Mosekilde E.* Coherent regimes of globally coupled dynamical systems // *Phys. Rev. Lett.* — 2003. — **90**.
15. *Tass P. A.* Phase resetting in medicine and biology. — Berlin: Springer, 1999.
16. *Maistrenko Yu. L., Popovych O. V., Tass P. A.* Desynchronization and chaos in the Kuramoto model // *Dynamics of Coupled Map Lattices and of Related Spatially Extended Systems (Lect. Notes Phys.)*. — 2005. — **671**. — P. 285–306.
17. *Popovych O. V., Maistrenko Yu. L., Tass P. A.* Phase chaos in coupled oscillators // *Phys. Rev. E*. — 2005. — **71**.
18. *Maistrenko Yu., Popovych O., Burylko O., Tass P.* Mechanism of desynchronization in the finite-dimensional Kuramoto model // *Phys. Rev. Lett.* — 2004. — **93**.
19. *Vasylenko A., Maistrenko Yu., Hasler M.* Modelling the phase synchronization in systems of two and three coupled oscillators // *Nonlinear Oscillations*. — 2004. — **7**, № 3. — P. 311–327.
20. *Arnol'd V.I., Afraimovich V.S., Il'yashenko Yu. S., Shilnikov L. P.* Dynamical systems. — Berlin: Springer, 1977.
21. *Liu Z., Lai Y.-C., Matias M. A.* Universal scaling of Lyapunov exponents in coupled chaotic oscillators // *Phys. Rev. E*. — 2003. — **67**.
22. *Nakagawa N., Kuramoto Y.* Anomalous Lyapunov spectrum in globally coupled oscillators // *Physica D*. — 1995. — **80**. — P. 307–316.

Received 01.06.07